Supporting Information for

Breaking Symmetry of Single-Atom Catalysts Enables Extremely Low Energy Barrier and High Stability for Large-Current-Density Water Splitting

Xueqin Mu,[†a,b] Xiangyao Gu, [†a,c] Shipeng Dai, [†a] Jiabing Chen, [†a] Yujia Cui,[a] Qu Chen,[a] Min Yu,[a] Changyun Chen,[a] Suli Liu,*[a] Shichun Mu*[b]

[a]Key Laboratory of Advanced Functional Materials of Nanjing, Nanjing Xiaozhuang University, Nanjing 211171, China.

[b]State Key Laboratory of Advanced Technology for Materials Synthesis and Processing, Wuhan University of Technology, Wuhan 430070, China.

[c]Guangxi Key Laboratory of Low Carbon Energy Materials, Guangxi Normal University, Guilin 541004, China.

[†]X. Q. Mu, X. Y. Gu, S. P. Dai and J. B. Chen contributed equally to this work.

*Corresponding E-mails: msc@whut.edu.cn; liusuli@njxzc.edu.cn

Experiment Section

Chemicals

2,5-Dihydroxyterephthalic acid (H$_4$DOT, 98%, Maklin), Iron(II) acetate (Fe(ac)$_2$, 90%, Energy Chemical), Cobaltous(II)nitrate hexahydrate (Co(NO$_3$)$_2$·6H$_2$O, ≥98.5%), N,N-Dimethyl formamide, RuCl$_3$·nH$_2$O.

Seawater was collected from the coast of Yellow Sea, China, and alkaline seawater was produced by adding KOH, until pH reached 12.7, and then insoluble precipitates were filtered by centrifugation.

Preparation of FeCo-LDH/NF

First, a piece of nickel foam (NF, 2 × 3 cm^2) was taken in anhydrous ethanol, 0.5 M HCl and deionized water, respectively, after ultrasonic treatment for 15min, the NF was vacuum-dried at 60°C. Next, 30 mL DMF was added into a teflon liner (50 mL) containing H$_4$DOT (0.090 g), Fe(ac)$_2$ (0.047 g), Co(NO$_3$)$_2$·6H$_2$O (0.210 g) to mix evenly, and then the 2 × 3 cm^2 NF after treatment was vertically dipped into the solution. The mixed reactor was reacted in the oven at 120 °C for 24 h. After the reaction, the solution was cooled to room temperature, the surface of the nickel foam was carefully washed with anhydrous ethanol, and then placed in 60 °C vacuum drying for 6 h to obtain FeCo-LDH/NF.

Preparation of Ru$_1$ SACs@FeCo-LDH/NF

The Ru$_1$ SACs@FeCo-LDH/NF were prepared at room temperature. First, 100 mg RuCl$_3$·nH$_2$O was dissolved in 25 mL methanol, and a piece of 2 × 3 cm^2 FeCo-LDH/NF was vertically immersed into the solution in a small beaker and reacted for 15 min. After the reaction, Ru$_1$ SACs@FeCo-LDH/NF was obtained by vacuum drying at 60 °C for 6 h.

Preparation of Ru$_2$ SACs@FeCo-LDH/NF

At the beginning, 100 mg RuCl$_3$·nH$_2$O was dissolved in teflon liner containing 25 mL methanol. After uniform mixing, a piece of 2 × 3 cm^2 FeCo-LDH/NF was vertically

immersed into the solution, and the high-pressure reactor was reacted at 130 °C for 3.5 h. When the reaction completed, the solution was cooled to room temperature, the surface of the nickel foam was carefully washed with anhydrous ethanol, and then placed in 60 °C vacuum drying for 6 h to obtain Ru_2 SACs@FeCo-LDH/NF.

Preparation of Ru/NF

As a comparison for Ru_1 SACs@FeCo-LDH/NF, the method is similar just change the FeCo-LDH/NF into 2×3 cm^2 pure NF, and other steps remain unchanged to obtain Ru/NF. In the same way, referring to the synthesis method of Ru_2 SACs@FeCo-LDH/NF that change the FeCo-LDH/NF into 2×3 cm^2 pure NF, and other steps remain unchanged to obtain the contrast sample.

Electrochemical characterization for OER

A three-compartment cell with O_2 saturated 1.0 M KOH solution was used for the electrochemical measurements with a 0.5×0.5 cm^2 Nickel foam grown in situ as the working electrode. Hg/HgO electrode and a Pt wire were used as the reference and the counter electrode, respectively. The potentials presented in this study are referred with respect to RHE. In this experiment, the potentiostatic method was used to test the stability of the samples. During the test, due to the excessive current, the water in the electrolyte rapidly evaporated, so it was necessary to replenish the water slowly at a regular time, so as not to destroy the pH of the electrolyte.

Electrochemical characterization for HER

A graphite rod was used as the counter electrode, the remaining steps are similar to OER testing. Keep the contact area of nickel foam same as the OER test and test in an electrolyte saturated with N_2.

Electrochemical characterization for water splitting

The electrochemical HER experiment was carried out on a CHI 660E electrochemical workstation (Shanghai, Chenhua Co.) with a standard two electrode system (1.0 M

KOH). Two same nickel foam with samples served as the positive and negative electrodes.

TOF

the turnover frequency (TOF) is supposed to be calculated according to the follow formula:[1,2]

$$TOF = \frac{j \times S}{a \times F \times n}$$

where j (mA cm^{-2}) is the measured current density at η =200 mV, S is the surface area of the electrode, a means the numbers of electrons transfer, F is the Faraday constant (96485.3 C mol^{-1}). This system calculates Co as the active site, and n is the mole of Co atoms coated on the electrode, the specific content is obtained by ICP test results.

Method and Model

The Co and Fe atoms embed FeCo-LDH (001), Co, Fe and Ru atoms embed Ru$_x$ SACs @FeCo-LDH (001) have been built. The atom ratio of Fe, Co, Ru in the calculation model was the same as validated experimentally by the ICP results (Table S1), the experimental ratio of Fe, Co, Ru (1:1.81:1.19) in Ru$_1$ SACs@FeCo-LDH is atomic ratio calculated by mass percentage. The ratio used in this system is 5:9:7= 1:1.8:1.4. Since continuous concentration changes cannot be achieved in the calculation model, it can only be as close to the experimental value as possible, which is impossible to be completely consistent. Moreover, the composition of the experimental sample will also have concentration fluctuations, so the proportion of the model can reflect the concentration trend of the experiment.[3-5]

The intermediates of OH, O and OOH groups have absorbed on Co or Fe or Ru atom. The bottom LDH atom layers were fixed and the top LDH atom layers were allowed to relax to the minimum in the enthalpy without any constraints. The first principles calculations in the framework of density functional theory, including structural, electronic performances, were carried out based on the Cambridge Sequential Total Energy Package known as CASTEP.[6] The exchange–correlation functional under the

generalized gradient approximation (GGA)[7] with norm-conserving pseudopotentials and Perdew–Burke–Ernzerhof functional was adopted to describe the electron–electron interaction.[8] An energy cutoff of 750 eV was used and a k-point sampling set of 7 x 7 x 1 were tested to be converged. A force tolerance of 0.01 eV Å^{-1}, energy tolerance of 5.0×10^{-7} eV per atom and maximum displacement of 5.0×10^{-4} Å were considered. The GGA+U with spin polarization was adopted to describe the localized d states,[9] where U = 3.42, 3.29 and 3.29 eV was applied for Co, Fe and Ru ions. The Grimme method for DFT-D correction is considered for all calculations.[10]

The calculation of the d-band center is based on the projected d-orbit $\rho_d(\epsilon)$, the specific calculation formula is:[11,12]

$$\in d = \frac{\int_{-\infty}^{\infty} \in \rho_d(\epsilon)d\epsilon}{\int_{-\infty}^{\infty} \rho_d(\epsilon)d\epsilon} \tag{1}$$

Fermi energy level is defined as the energy zero point, that is, the energy of d-band is relative to Fermi energy level.

Adsorption energy ΔE of A = OH, O and OOH groups on the surface of substrates was defined as:[6]

$$\Delta E = E_{*A} - (E_* + E_A) \tag{2}$$

where *A and * denote the adsorption of A groups on substrates and the bare substrates, E_A denotes the energy of A groups.

Free energy change ΔG of the reaction was calculated as the difference between the free energies of the initial and final states as shown below:[13,14]

$$\Delta G = \Delta E + \Delta ZPE - T\Delta S \tag{3}$$

where ΔE is the energy change between the reactant and product obtained from DFT calculations; ΔZPE is the change of zero point energy; T and ΔS denote temperature and change of entropy, respectively. In here, T = 300K was considered.

1. H. You, D. Wu, D. Si, M. Cao, F. Sun, H. Zhang, H. Wang, T. Liu and R. Cao, *J. Am. Chem. Soc.*, 2022, **144**, 9254-9263.

2. F. Zheng, Z. Zhang, D. Xiang, P. Li, C. Du, Z. Zhuang, X. Li and W. Chen, *J. Colloid Interface Sci.,* 2019, **555**, 541-547.

3. S. Liu, Q. Zhang, Y. Li, M. Han, L. Gu, C. Nan, J. Bao and Z. Dai, *J. Am. Chem. Soc.,* 2015, **137**, 2820-2823.

4. Y. Zhu, J. Peng, X. Zhu, L. Bu, Q. Shao, C. Pao, Z. Hu, Y. Li, J. Wu and X. Huang, *Nano Lett.*, 2021, **21**, 6625-6632.

5. Z. Luo, Y. Zhou, X. Hu, N. Kane, T. Li, W. Zhang, Z. Liu, Y. Ding, Y. Liu and M. Liu, *Energy Environ. Sci.*, 2022, **15**, 2992-3003.

6. M. Segall, P. Probert, C. Pickard, P. Hasnip, S. Clark and M. Payne, *J. Phys.: Condens. Matter*, 2002, **14**, 2717.

7. J. Perdew, K. Burke and M. Ernzerhof, Phys. Rev. Lett., 1996, **77**, 3865.

8. D. Hamann, M. Schlüter and C. Chiang, *Phys. Rev. Lett.*, 1979, **43**, 1494.

9. H. Xu, D. Cheng, D. Cao and X. Zeng, Nat. Catal., 2018, **5**, 339-348.

10. S. Grimme, *J. Comput. Chem.*, 2006, **27**, 1787-1799.

11. B. Hammer, J. K. Norskov, *Nature*, 1995, **376**, 238-240.

12. B. Hammer, J. K. Nørskov, *Surf. Sci.*, 1995, **343**, 211-220.

13. H. Li, Y. Wu, C. Li, Y. Gong, L. Niu, X. Liu, Q. Jiang, C. Sun and S. Q. Xu, *Appl. Catal. B: Environ.*, 2019, **251**, 305-312.

14. M. Bajdich, M. García-Mota, A. Vojvodic, J. K. Nørskov and A. T. Bell, *J. Am. Chem. Soc.*, 2013, **135,** 13521-13530.

Table S1. The mass percentage from ICP analysis for different samples.

Mass%	Ru₁ SACs@FeCo-LDH	Ru₂ SACs@FeCo-LDH	FeCo-LDH
Ru	30%	96.7%	-
Fe	25%	1.51%	27.0%
Co	45%	0.23%	73.0%
atomic ratio	Fe:Co:Ru=1:1.81:1.19	Fe:Co:Ru=1:0.15:65	Fe:Co = 1:2.7
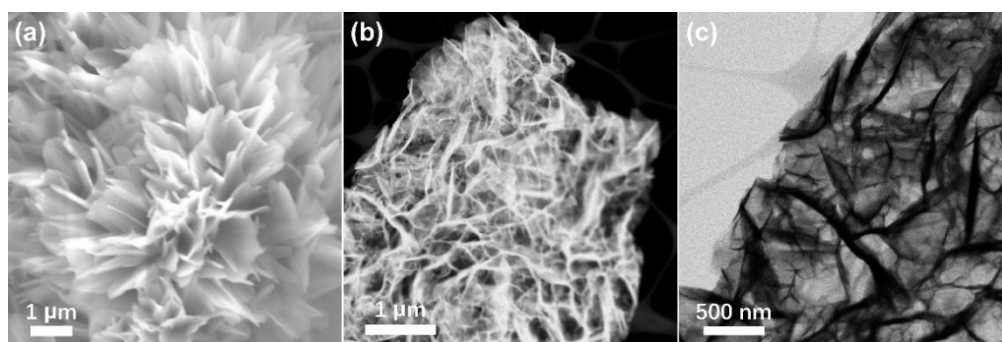
Figure S1. (a) SEM, (b) STEM and (c) TEM images of Ru₁ SACs@FeCo-LDH.
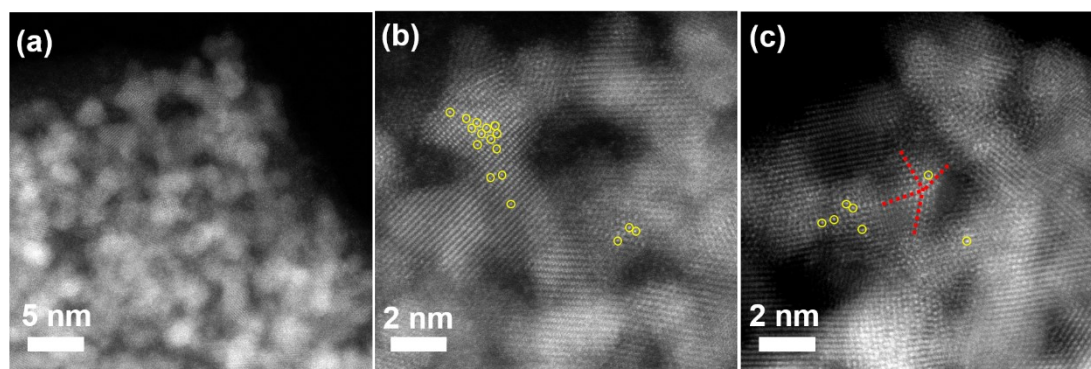
Figure S2. (a) SEM, (b) STEM and (c) TEM images of Ru₂ SACs@FeCo-LDH.
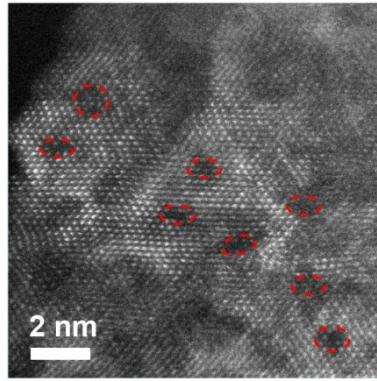
Figure S3. HAADF-STEM image for Ru_1 SACs@FeCo-LDH.
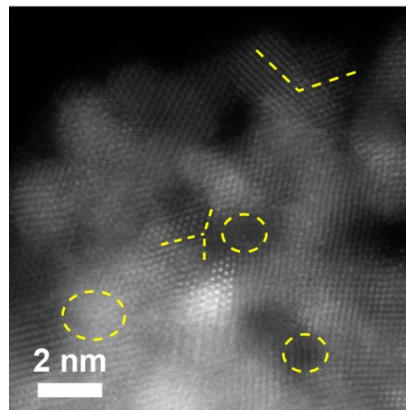
Figure S4. HAADF-STEM image for Ru_2 SACs@FeCo-LDH.
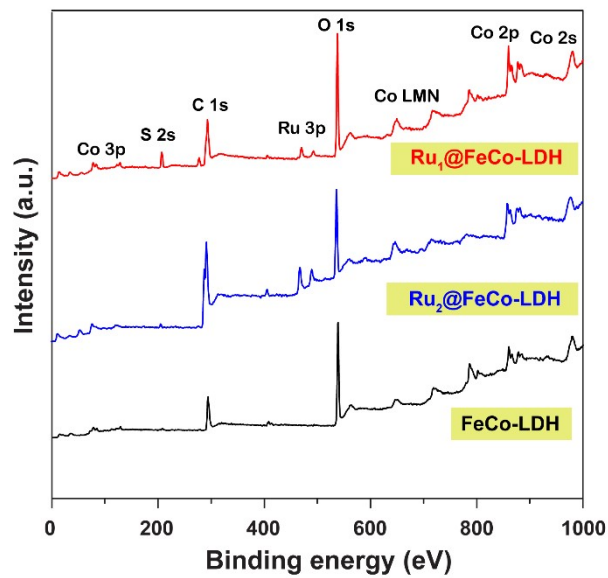
Figure S5. XPS spectra of Ru_1 SACs@FeCo-LDH, Ru_2 SACs@FeCo-LDH and FeCo-LDH, respectively.

Table S2. The elemental atomic percentage from XPS analysis for different samples.

Atomic%(XPS)	Ru$_1$ SACs@FeCo-LDH	Ru$_2$ SACs@FeCo-LDH	FeCo-LDH
Ru	3.28%	3.43%	-
O	72.98%	80.69%	77.79%
Fe	5.64%	4.48%	6.11%
Co	4.79%	1.46%	7.78%
Ni	13.31%	9.94%	8.32%
atomic ratio	Fe:Co:Ru=1:0.85:0.58	Fe:Co:Ru=1:0.33:0.77	Fe:Co=1:1.27
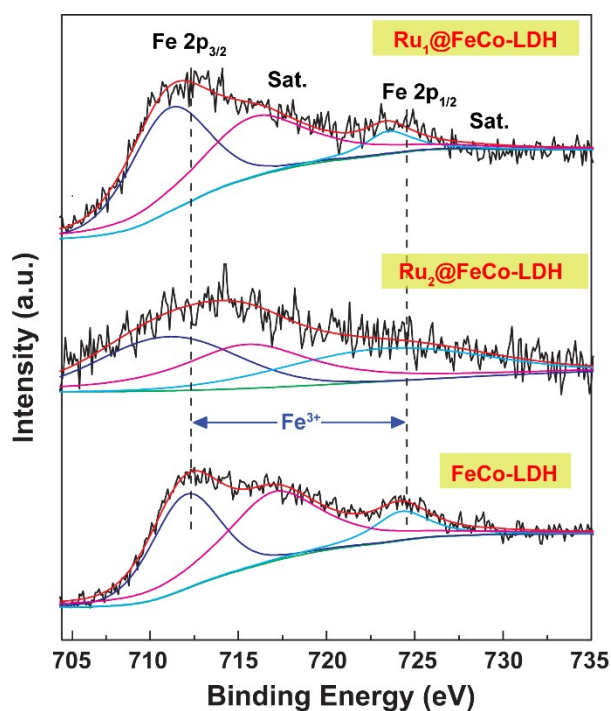
Figure S6. Fe 2p XPS spectra of Ru$_1$ SACs@FeCo-LDH and FeCo-LDH, respectively.
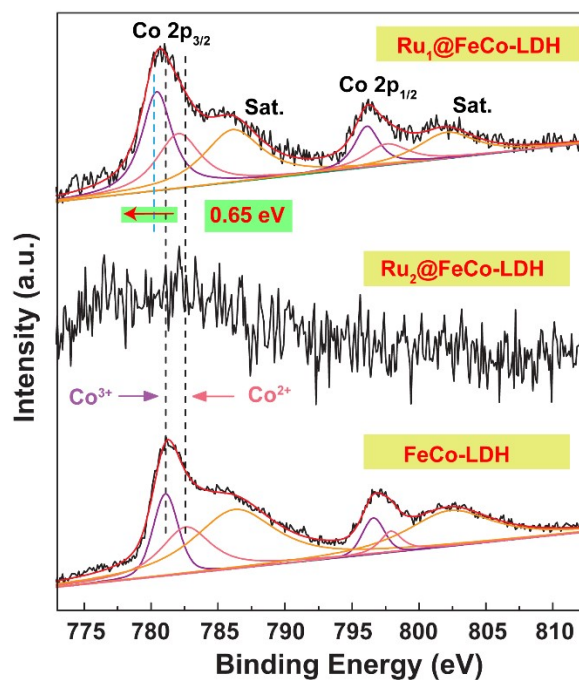
Figure S7. Co 2p XPS spectra of Ru_1 SACs@FeCo-LDH and FeCo-LDH, respectively.
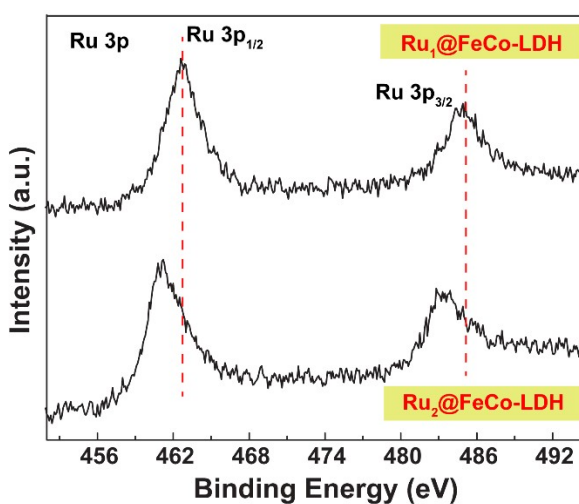
Figure S8. Ru 3p XPS spectra of Ru_1 SACs@FeCo-LDH and Ru_2 SACs@FeCo-LDH, respectively.
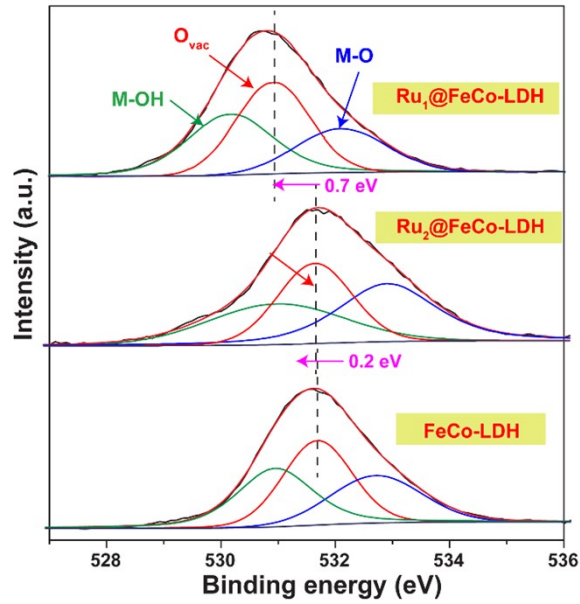
Figure S9. O 1s XPS spectra of Ru_1 SACs@FeCo-LDH, Ru_2 SACs@FeCo-LDH and FeCo-LDH, respectively.
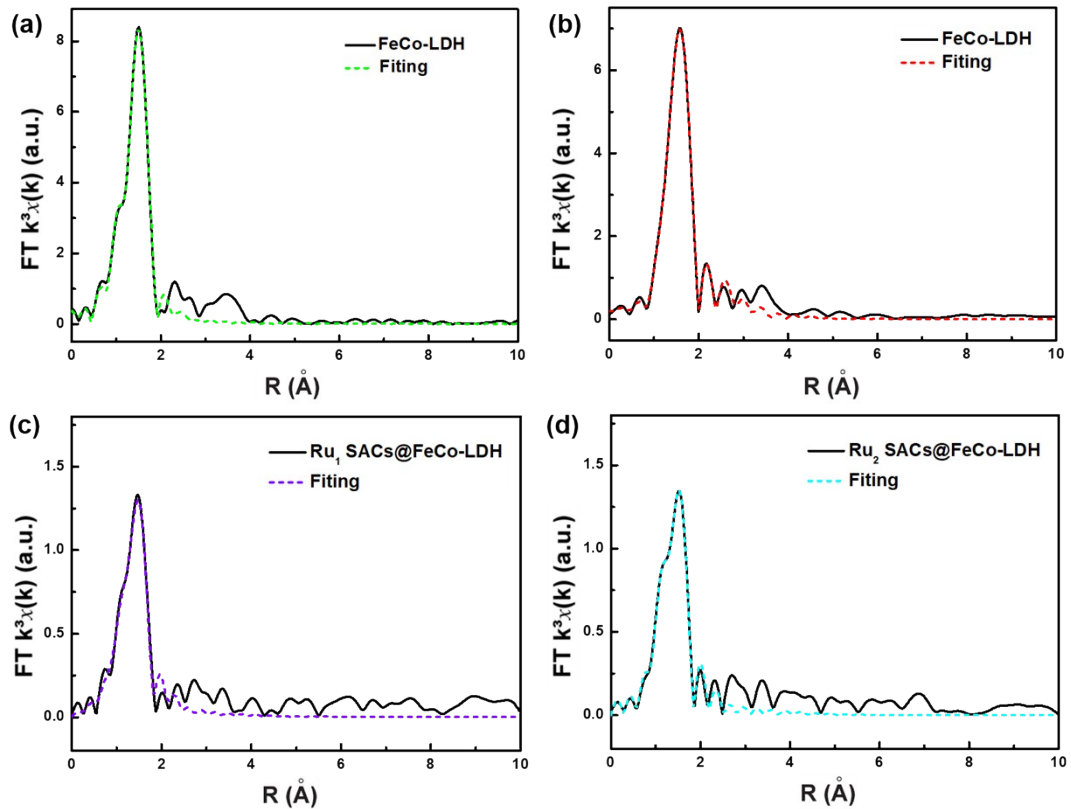
Figure S10. EXAFS fitting curve of (a) Fe and (b) Co K-edge for FeCo-LDH, Ru K-edge for (c) Ru_1 SACs@FeCo-LDH and (d) Ru_2 SACs@FeCo-LDH in R space, respectively.

Table S3. Structural parameters extracted from the Fe and Co K-edge EXAFS fitting. (S_0^2=0.86 for Fe, S_0^2=0.83 for Co, S_0^2=0.83 for Ru)

Samples	Scattering pair	CN	R(Å)	$\sigma^2(10^{-3}Å^2)$	ΔE_0(eV)	R factor
Ru$_1$ SACs@FeCo-LDH	Fe-C/N/O	4.2	1.91	4.7	1.5	0.009
	Co-C/N/O	4.1	2.96	4.8	2.0	0.005
	Ru-C/N/O	4.2	1.98	4.9	1.5	0.006
FeCo-LDH	Fe-C/N/O	3.8	1.93	5.7	1.5	0.006
	Co-C/N/O	4.0	1.97	4.4	2.0	0.008
Ru$_2$ SACs@FeCo-LDH	Ru-C/N/O	4.3	2.01	5.7	1.5	0.009

S_0^2 is the amplitude reduction factor; CN is the coordination number; R is interatomic distance (the bond length between central atoms and surrounding coordination atoms); σ^2 is Debye-Waller factor (a measure of thermal and static disorder in absorber-scatterer distances); ΔE_0 is edge-energy shift (the difference between the zero kinetic energy value of the sample and that of the theoretical model). R factor is used to value the goodness of the fitting.

Error bounds that characterize the structural parameters obtained by EXAFS spectroscopy were estimated as N ± 20%; R ± 1%; σ^2 ± 20%; ΔE_0 ± 20%.
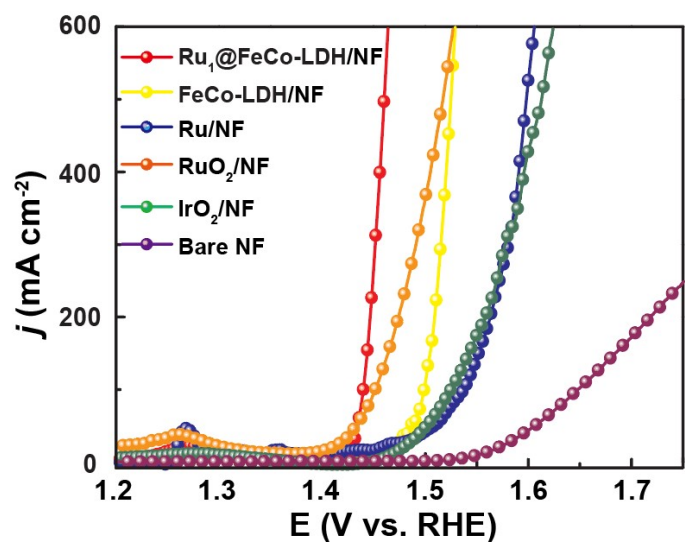
Figure S11. Polarization curves in 1.0 M KOH for OER electrocatalysis.

Table S4. Comparison of OER activities of other catalysts in KOH solution.

Catalysts	η at 500 mA cm^{-2} (mV)	Reference
Ru$_1$ SACs@FeCo-LDH	**230@500** **246@1000**	**This work**
NiMoO$_x$/NiMoS	278@500 334@1000	*Nat. Commun.*, 2020, **11**, 5462.
MoNi$_4$/SSW‖SSW Rs-12h	285@500	*Adv. Energy Mater.*, 2020, **10**, 1904020.
Ni$_3$Nb-doped NiFe-OOH	236@500 249@1000	*Adv. Energy Mater.*, 2021, **11**, 2100968.
Ru-CoO$_x$/NF	370@1000	*Small*, 2021, **17**, 2102777.
Ni$_{0.8}$Fe$_{0.2}$-AHNA	260 @1078	*Energy Environ. Sci.*, 2020, **13**, 86-95.
FeP/Ni$_2$P	293 @1000	*Nat. Commun.*, 2018, **9**, 2551.
F$_{0.25}$C$_1$CH/NF	308 @1000	*Adv. Energy Mater.*, 2018, **8**, 1800175.
nano-KFO/NF	308 @100 421 @2000	*J. Mater. Chem. A*, 2021, **9**, 7586-7593.
5h-ANF	350 @500	*ACS Nano*, 2021, **15**, 3468-3480.
Fe-CoP/NF	295 @500 428 @1000	*Adv. Sci.*, 2018, **5**, 1800949.
(Ni,Fe)OOH	259 @500 289 @1000	*Energy Environ. Sci.*, 2018, **11**, 2858-2864.
NFN-MOF/NF	360 @500	*Adv. Energy Mater.*, 2018, **8**, 1801065.
SSW Rs-12 h	287 @500	*Adv. Energy Mater.*, 2020, **10**, 1904020.
Ni$_3$S$_2$/Fe-NiP$_x$/NFc	270 @500 291 @1000	*Adv. Sci.*, 2022, **9**, 2104846.
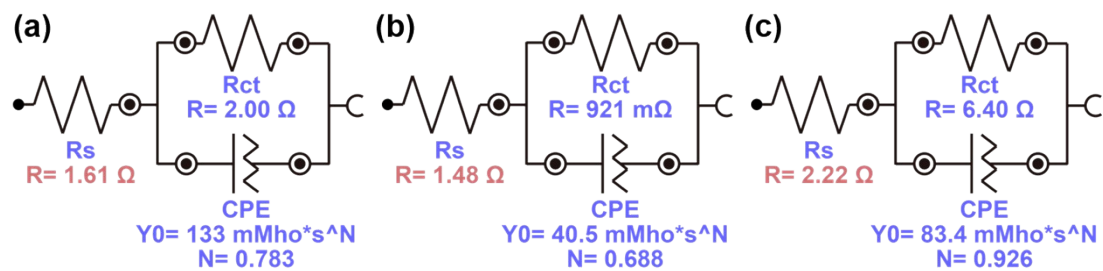
Figure S12. The equivalent circuit of (a) Ru_1 SACs@FeCo-LDH, (b) FeCo-LDH and (c) Ru/NF electrocatalysts in 1.0 M KOH solution, respectively.
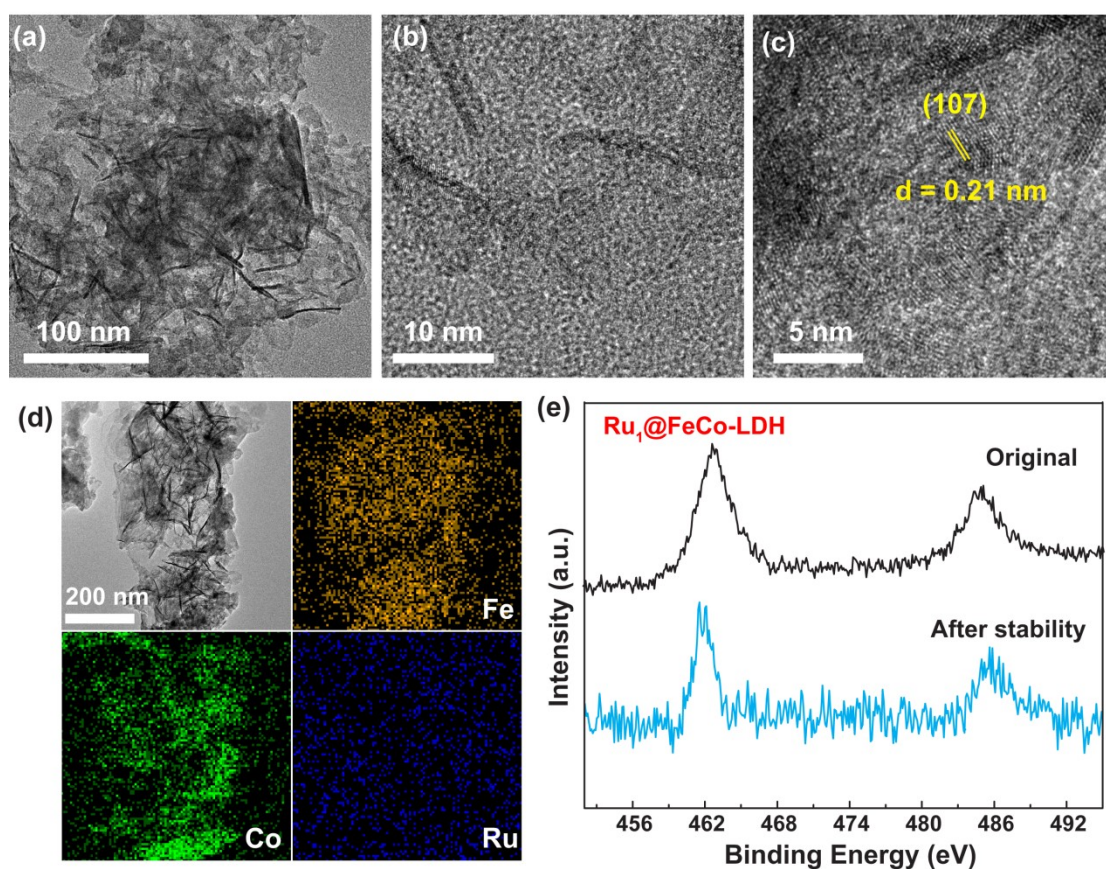
Figure S13. (a) TEM, (b, c) HRTEM images and (d) elemental mapping images after the stability test. (e) Ru 3p XPS spectra before and after the stability test, respectively.
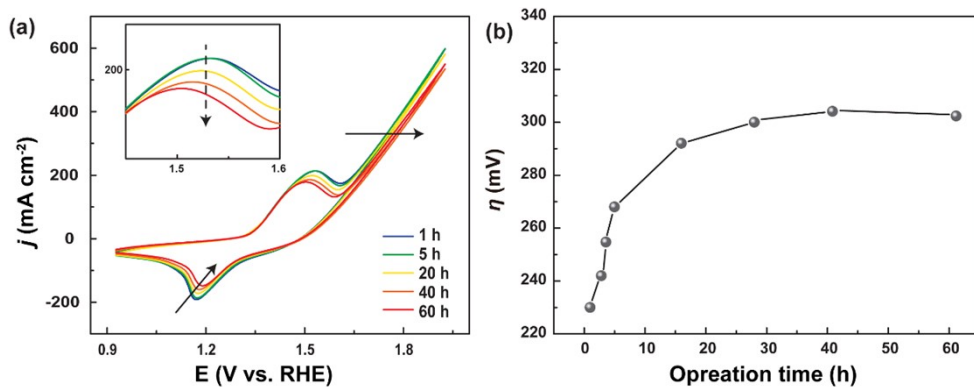
Figure S14. (a) CV curves and (b) the plot of the extracted corresponding overpotential at a current density of 10 mA cm^{-2} in the backward sweep in (a) of Ru$_1$ SACs@FeCo LDH catalyst along with the operation time.
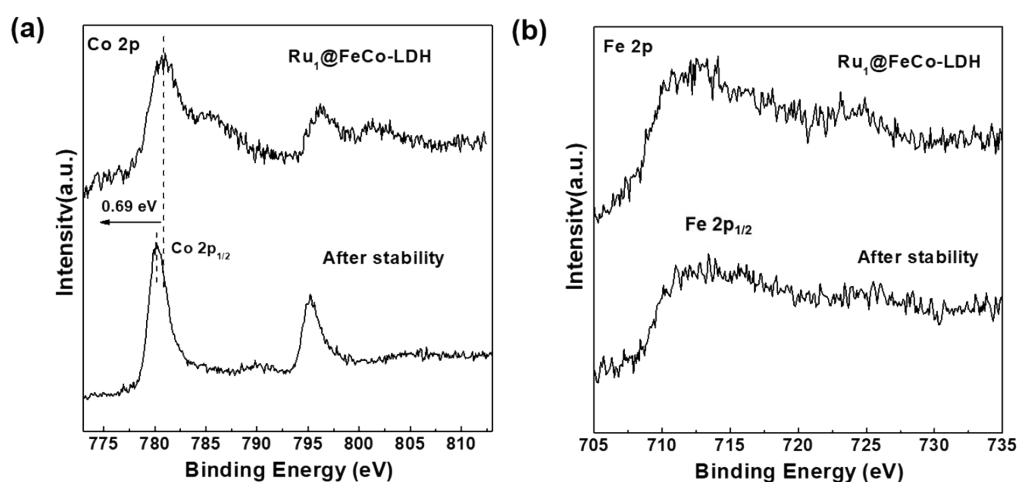
Figure S15. (a) Co 2p and (b) Fe 2p XPS spectra of Ru$_1$ SACs@FeCo-LDH and after 1200 h, respectively.
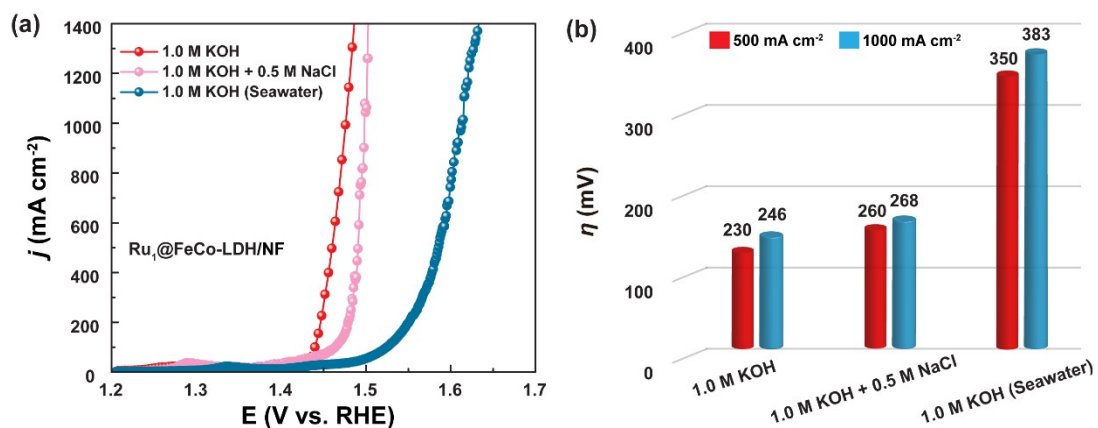
Figure S16. (a) Polarization curves and (b) comparison of the overpotentials required to achieve current densities of 500 and 1000 mA cm^{-2} for the Ru$_1$ SACs@FeCo LDH electrode tested in different electrolytes, respectively.
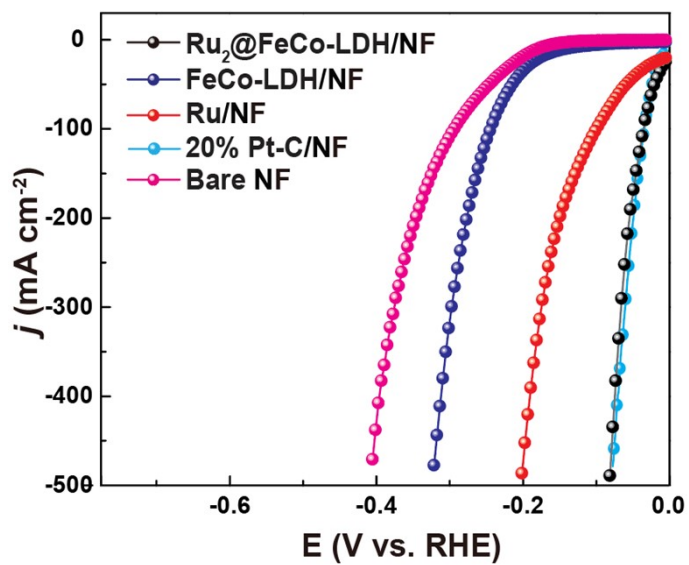
Figure S17. Polarization curves in 1.0 M KOH for HER electrocatalysis.

Table S5. Comparison of HER activities of other catalysts in KOH solution.

Catalysts	η at 500 mA cm^{-2} (mV)	Reference
Ru$_2$ SACs@FeCo-LDH	**84@500** **117@1000**	**This work**
(Ni,Fe)OOH	259 @500 289 @1000	*Energy Environ. Sci.*, 2018, **11**, 2858-2864.
NFN-MOF/NF	293 @500	*Adv. Energy Mater.*, 2018, **8**, 1801065.
Pt@ Cu-0.3	438 @1000	*Adv. Funct. Mater.*, 2021, **31**, 2105579.
Ni-Mo-B HF	257 @500	*Adv. Funct. Mater.*, 2021, **32**, 2107308.
Ni$_3$Nb doped NiFe-OOH	236 @500 249 @1000 261 @2000	*Adv. Energy Mater.*, 2021, **11**, 2100968.
Ni$_2$P/NF	306 @1000 368 @ 1500	*J. Am. Chem. Soc.*, 2019, **141**, 7537.
h-NiMoFe	97 @1000	*Energy Environ. Sci.*, 2021, **14**, 4610.
F$_{0.25}$C$_1$CH/NF	256 @1000	*Adv. Energy Mater.*, 2018, **8**, 1800175.
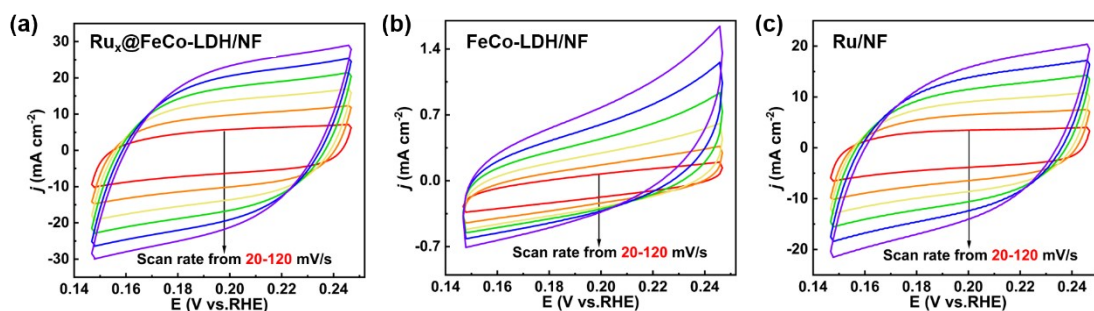
Figure S18. Cyclic voltammograms of (a)-(c) of Ru$_2$ SACs@FeCo-LDH, FeCo-LDH and Ru/NF electrocatalysts at various scan rates, respectively.
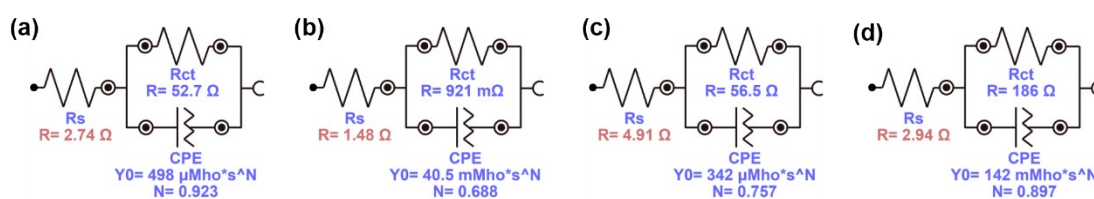
Figure S19. The equivalent circuit of (a) Ru$_2$ SACs@FeCo-LDH, (b) FeCo-LDH, (c) Ru/NF and (d) Bare NF electrocatalysts, respectively.
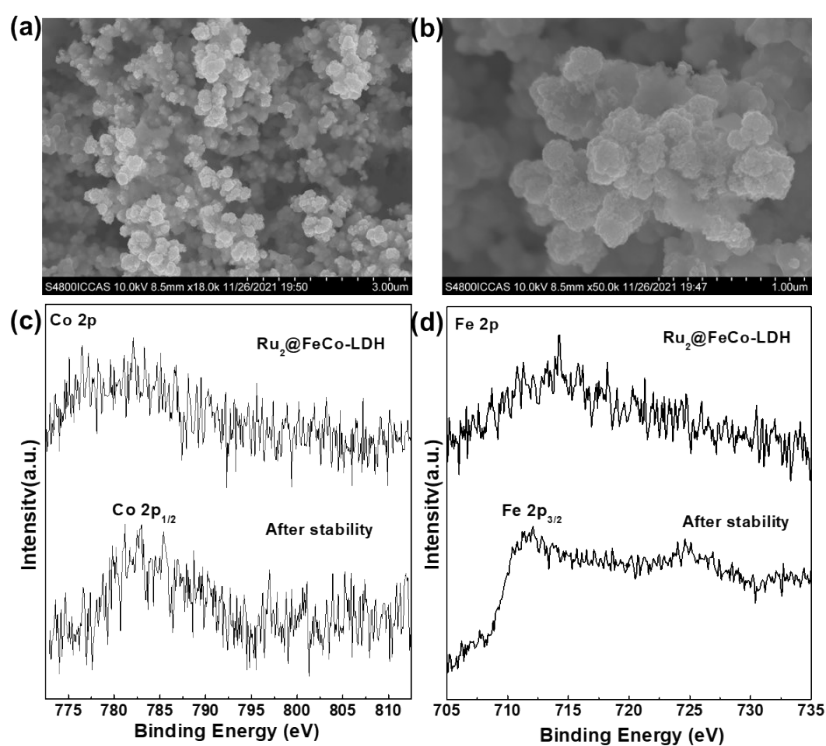
Figure S20. (a, b) SEM images, (c)Co 2p and (d) Fe 2p XPS spectra of Ru$_2$ SACs@FeCo-LDH and after 1000 h.

Figure S21. (a) Schematic of the electrolyzed water reaction. (b) H_2 (Green) and O_2 (Red) generated at 5, 10, 15, 20 min, respectively.

Table S6. Comparison of OWS activities of other catalysts in KOH solution.

Catalysts	Voltage (V) at mA cm^{-2}	Reference
Ru$_x$ SACs@FeCo-LDH	**1.47 @500** **1.52 @1000**	**This work**
(Ni,Fe)OOH // MoNi$_4$	1.586 @500 1.657 @1000	*Energy Environ. Sci.*, 2018, **11**, 2858-2864.
NFN-MOF/NF	1.96 @500	*Adv. Energy Mater.*, 2018, **8**, 1801065.
Ni nanowire array(−)//Ni$_{0.8}$Fe$_{0.2}$-AHNA(+)	1.70 @500	*Energy Environ. Sci.*, 2020, **13**, 86-95.
Ni-Mo-B HF	1.88 @500	*Adv. Funct. Mater.*, 2021, **32**, 2107308.
FeP/Ni$_2$P	1.72 @500 1.78 @1000	*Nat. Commun.*, 2018, **8**, 2551.
FeCo carbonate hydroxide	1.52 @500	*Adv. Energy Mater.*, 2018, **8**, 1800175.
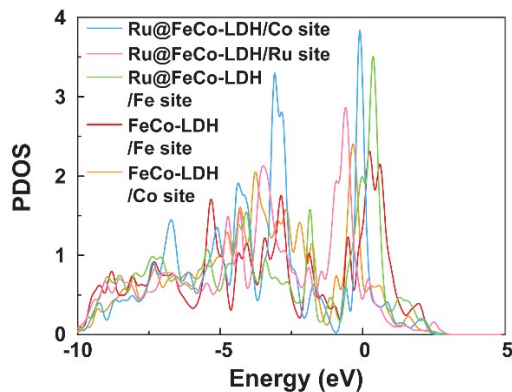
Figure S22. PDOS of Fe, Co and Ru active sites over the Ru SACs@FeCo-LDH and FeCo-LDH. respectively.
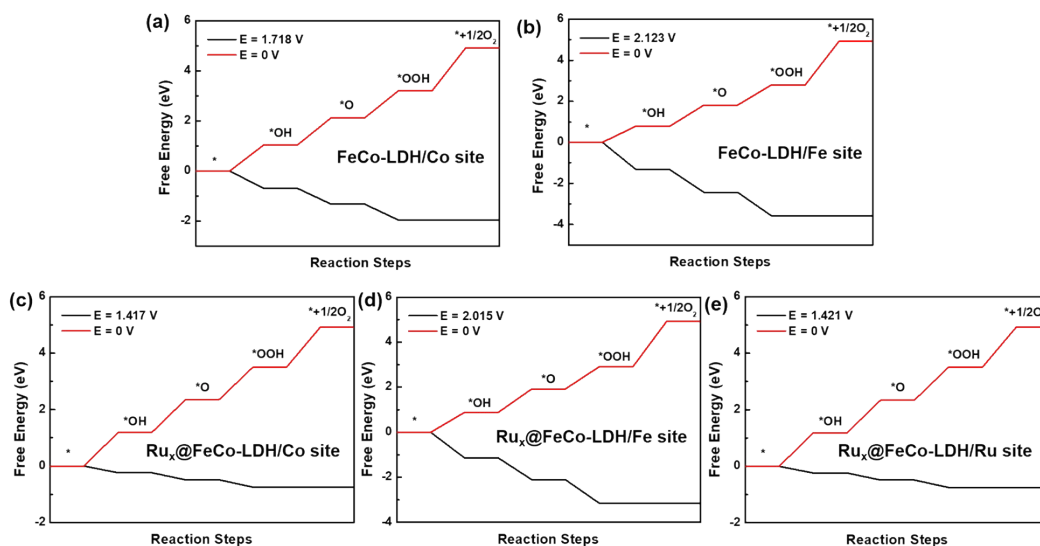
Figure S23. (a-b) Energy profile for the OER process on the FeCo-LDH and (c-e) Ru_x SACs@FeCo-LDH, respectively.
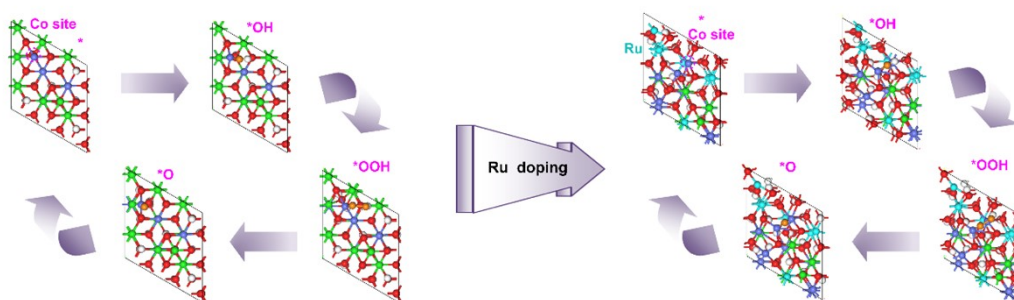
Figure S24. Top view of representative OER mechanism on Co active site over the FeCo-LDH and Ru_x SACs@FeCo-LDH, respectively.
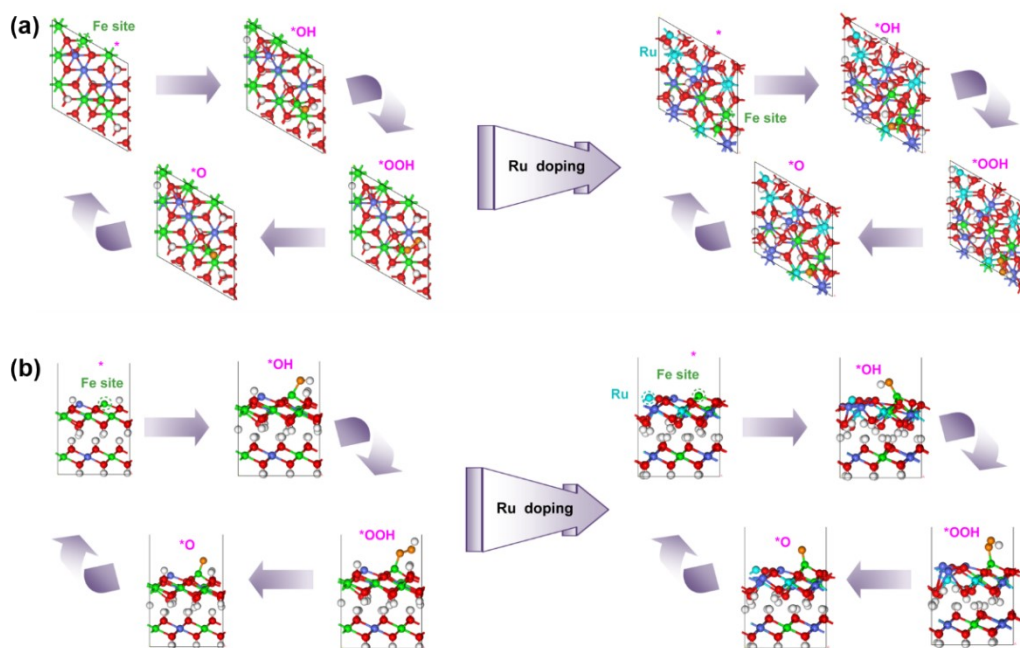
Figure S25. (a) Top and (b) side view of representative OER mechanism on Fe active site over the FeCo-LDH and Ru$_x$ SACs@FeCo-LDH, respectively.
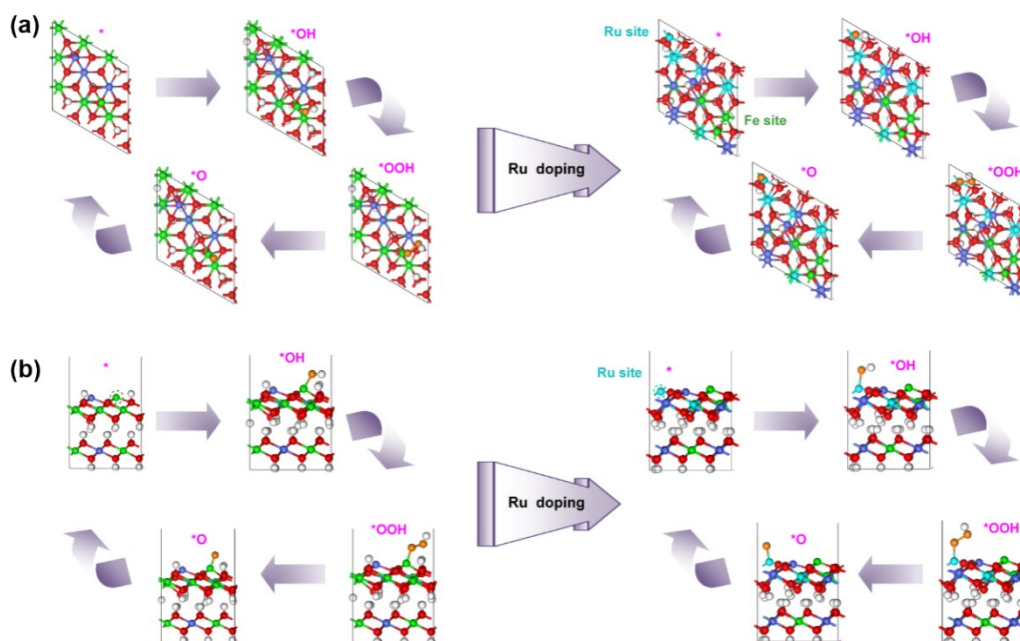
Figure S26. (a) Top and (b) side view of representative OER mechanism on Ru active site over the FeCo-LDH and Ru$_x$ SACs@FeCo-LDH, respectively.